Placenta 77 (2019) 1–7

Contents lists available at ScienceDirect

Placenta

journal homepage: www.elsevier.com/locate/placenta

Pre-clinical magnetic resonance imaging of retroplacental clear space throughout gestation

Andrew A. Badachhape[a,b], Aarav Kumar[b], Ketan B. Ghaghada[b], Igor V. Stupin[b], Mayank Srivastava[b], Laxman Devkota[b,c], Zbigniew Starosolski[b,c], Eric A. Tanifum[b], Verghese George[b], Karin A. Fox[d], Chandrasekhar Yallampalli[d], Ananth V. Annapragada[b,*]

[a] Department of Radiology, Baylor College of Medicine, Houston, TX, 77030, USA
[b] The Singleton Department of Pediatric Radiology, Texas Children's Hospital, Houston, TX, 77030, USA
[c] Baylor College of Medicine, Houston, TX, 77030, USA
[d] Department of Obstetrics and Gynecology, Texas Children's Hospital, Houston, TX, 77030, USA

ARTICLE INFO

Keywords:
Abnormally invasive placenta
Accreta
Magnetic resonance imaging
Liposomal-Gd blood pool contrast agent
Retroplacental space

ABSTRACT

Introduction: Visualization of the retroplacental clear space (RPCS) may provide critical insight into the development of *abnormally invasive placenta* (AIP). In this pre-clinical study, we characterized the appearance of the RPCS on magnetic resonance imaging (MRI) during the second half of gestation using a liposomal gadolinium contrast agent (liposomal-Gd).

Materials and methods: Studies were performed in fifteen pregnant C57BL/6 mice at 10, 12, 14, 16, and 18 days of gestation. MRI was performed on a 1T permanent magnet scanner. Pre-contrast and post-contrast images were acquired using T1-weighted gradient-recalled echo (T1w-GRE) and T2-weighted fast spin echo (T2w-FSE) sequences. Animals were euthanized after imaging and feto-placental units harvested for histological examination. Visualization of the RPCS was scored by a maternal-fetal radiologist and quantified by measuring the contrast-to-noise ratio (CNR) on T1w images. Feto-placental features were segmented for analysis of volumetric changes during gestation.

Results: Contrast-enhanced T1w images enabled the visualization of structural changes in placental development between days 10–18 of gestation. Although the placental margin on the fetal side was clearly visible at all time points, the RPCS was partially visible at day 10 of gestation, and clearly visible by day 12. Hematoxylin and eosin (H&E) staining of the placental tissue corroborated MRI findings of structural and morphological changes in the placenta.

Conclusions: Contrast-enhanced MR imaging using liposomal-Gd enabled adequate visualization of the retroplacental clear space starting at day 12 of gestation. The agent also enabled characterization of placental structure and morphological changes through gestation.

1. Introduction

Abnormally Invasive Placenta (AIP) is a gestational condition where the placenta invades the uterine wall, thus complicating delivery. AIP has three primary variants: 1) accreta, where the placental tissue extends beyond the decidua basalis 2) increta, where the placenta grows into the uterine myometrium, and 3) perceta, where the placenta invades through the myometrium and uterine serosa, and sometimes into adjacent organs [1]. The incidence of overly invasive placental development has increased significantly over the past fifty years, including a near 10-fold increase in the incidence of AIP over the last 30 years [2]. Diagnosis of AIP remains challenging; ultrasound is employed in the setting of known risk factors, with MRI used under special circumstances [3]. While aggressive placental invasion seen in increta or perceta may be detected with relative ease through traditional imaging, more subtle abnormalities related to accreta are harder to visualize,

* Corresponding author. The Singleton Department of Pediatric Radiology, Texas Children's Hospital, 1102 Bates Street, Suite 850, Houston, TX, 77030, USA.
E-mail addresses: badachha@bcm.edu (A.A. Badachhape), kumar.aarav2002@gmail.com (A. Kumar), kbghagha@texaschildrens.org (K.B. Ghaghada), ivstupin@texaschildrens.org (I.V. Stupin), mxsrivas@texaschildrens.org (M. Srivastava), laxman.devkota@bcm.edu (L. Devkota), zbigniew.starosolski@bcm.edu (Z. Starosolski), eatanifu@texaschildrens.org (E.A. Tanifum), vxgeorge@texaschildrens.org (V. George), kafox@bcm.edu (K.A. Fox), chandrasekhar.yallampalli@bcm.edu (C. Yallampalli), avannapr@texaschildrens.org (A.V. Annapragada).

https://doi.org/10.1016/j.placenta.2019.01.017
Received 20 August 2018; Received in revised form 16 January 2019; Accepted 21 January 2019

even with MRI [4]. Sensitivity of detection on MRI with junior readers is < 80% overall while specificity is typically high (88%), indicating that a significant fraction of AIP cases go undetected prenatally [5].

A method to definitively identify and characterize the extent of placental invasion is highly desirable. With ultrasound, placental invasion is diagnosed through multiple abnormal findings including distortion of the bladder interface, irregularly shaped hypoechoic spaces, or "lacunae", seen within the placenta, hypervascularity on color Doppler, or an abnormal bulge of placental tissue beyond the borders of the myometrium [6–8]. Additionally, under normal conditions, a healthy utero-placental interface is characterized by a hypoechoic region known as the retroplacental clear space [9]. The sensitivity and specificity of ultrasound for AIP can range widely based on the experience of the observer [6]. In large population-based studies using only ultrasound from a wide variety of clinical settings (not limited only to tertiary centers) antenatal detection may be as low as 50%, [2,10] thus MRI has seen increased use to confirm ultrasound findings or provide further characterization of the condition [3,11–13]. Guidelines proposed by the American Congress of Obstetricians and Gynecologists (ACOG) recommend use of MRI as an adjunct in the case of unclear ultrasound readings, particularly in cases of posterior placental location [14]. With conventional non-contrast MRI, indirect signs such as increased placental vascularity and T2-dark placental bands are used to identify AIP, and are especially helpful in identifying cases of deep invasion [9,11,15]. However, the study does not usually demonstrate a retroplacental space that demarcates the uteroplacental interface. Direct visual confirmation of an abnormal placental-uterine interface is desirable, especially to clearly delineate normal from adherent or only focally invasive placentas. Recent MR studies of invasive placentation have demonstrated the effectiveness of using gadolinium (Gd) based contrast agents to improve visualization of this interface in both clinical [16] and preclinical [17] applications.

While contrast-enhanced MRI may improve diagnostic accuracy of AIP, concerns over fetal exposure to Gd have limited its use clinically. In pregnant women, retrospective clinical studies have attempted to focus on the safety of both the mother and fetus. Among these studies, the consensus is that Gd agents pose little to no risk to the mother but is less conclusive about the safety profile for the fetus. For instance, one comprehensive review of the clinical use and safety of Gd has demonstrated the overall low adverse risk of Gd contrast agents to both mother and fetus [18]. Additionally, this review notes several studies, including one by Ray et al. of 1.4 million deliveries in the Canadian province of Ontario, where fetal exposure to Gd in the first trimester resulted in no adverse neonatal outcomes [19]. However, the study by Ray et al. noted an increase in the risk for neonatal rheumatologic and inflammatory conditions, and even stillbirth, when Gd exposure occurs during the 2nd or 3rd trimester [19]. Current clinically approved Gd contrast agents are not absolutely contraindicated in pregnancy, but their use is evaluated on a case-by-case basis, considering the risk-benefit ratio. Yet, even these agents do not adequately facilitate clear visualization of the RPCS [17]. The potential risks to the fetus necessitate investigations into a contrast agent that does not diffuse across the placental barrier.

Previous work by our group demonstrated that a long circulating, liposomal-Gd blood-pool contrast agent does not penetrate the placental barrier in rodent models [17,20]. Further, we demonstrated the superior performance of the liposomal-Gd contrast agent, when compared to a conventional macrocylic-based Gd contrast agent, for *in vivo* visualization of placental margins and the retroplacental clear space, albeit at a single, late time point during gestation [17].

In this pre-clinical study, we characterized the appearance and development of the retroplacental clear space in MRI through the second half of gestation in a pregnant mouse model using a liposomal-Gd contrast agent. A secondary goal of this study was to determine the earliest time point at which the retroplacental clear space could be clearly visualized using contrast-enhanced MRI. Imaging was performed on a 1T permanent magnet small animal MRI thus providing insight into the expected conspicuity and signal at clinically-relevant field strengths.

2. Materials and Methods

All animal studies were performed under a protocol approved by the Institutional Animal Care and Use Committee of the Baylor College of Medicine. The studies were in compliance with NC3RS-ARRIVE guidelines.

2.1. Animal model

Fifteen pregnant female C57BL/6J mice (8–12 weeks old; ~20–30 g body weight before pregnancy) were used in the study. To ensure that there was no residual contrast signal in subsequent time points, different cohorts of pregnant animals were imaged at each of the five gestational ages (n = 3 pregnant animals per cohort per time point). The first day of gestation, designated as 0.5, was when a vaginal copulation plug was detected. Imaging was performed on days 10.5, 12.5, 14.5, 16.5, and 18.5 of pregnancy (referred to hereafter as E10.5, E12.5, E14.5, E16.5, and E18.5). Since each animal bore between 7 and 10 fetoplacental units (FPU), we were able to analyze 23 to 28 FPU at each time point.

2.2. Liposomal-Gd contrast agent

Liposomal-Gd contrast agent was prepared as per procedures described previously [17]. Briefly, hydrogenated soy phosphatidylcholine (HSPC), 1,2-distearoyl-sn-glycero-3-phosphoethanolamine 1,4,7,10-Tetraazacyclododecane-1,4,7,10-tetraacetic acid Gadolinium (III) (DSPE-DOTA-Gd), Cholesterol and 1,2-distearoyl-sn-glycero-3-phosphoethanolamine-N-[methoxy(- poly(ethylene glycol))-2000] (mPEG2000-DSPE) were dissolved in t-butanol at a molar ratio 31.5:25:40:3.5. The lipid solution was hydrated with 150 mM NaCl/10 mM histidine to achieve a lipid concentration of 75 mM. The solution was stirred for 30 min at 60C and then sequentially extruded on a Lipex Thermoline extruder to size the liposomes to ~150 nm. The resulting solution was dialyzed against 150 mM NaCl/10 mM histidine. The mean liposome size in the final formulation, determined by dynamic light scattering (DLS), was 112 nm with a poly-dispersity index of less than 0.15. The gadolinium and phospholipid (equivalent phosphorus) concentrations in the liposomal formulation, quantified using inductively coupled plasma optical emission spectroscopy (ICP-OES), were 13 mM and 33 mM, respectively. Liposomal-Gd contrast agent exhibits a long half-life (17.5 ± 1.5 h) [17,20,21] and T1 relaxivity is $31 \pm 5\,(s{\cdot}mM)^{-1}$ [22]. For *in vivo* studies, liposomal-Gd was administered intravenously via the tail vein at a dose of 0.1 mmol Gd/kg body weight.

2.3. Magnetic resonance imaging (MRI)

Imaging was performed on a 1T permanent MRI scanner (M2 system, Aspect Imaging, Shoham, Israel), incorporating a 35 mm transmit-receive RF volume coil.

Animals were sedated using 3% isoflurane, placed on the MRI animal bed, and then maintained at 1–2% isoflurane delivered using a nose cone setup. Respiration rate was monitored by a pneumatically controlled pressure pad placed underneath the abdominal region of the animals.

All animals underwent pre-contrast and post-contrast scans. T1-weighted (T1w) scans were acquired using a 3D gradient echo sequence (GRE). Post-contrast scans were initiated ~5 min post injection and < 1 h after pre-scans. Scan parameters for T1w-GRE sequence were: echo time (TE) = 3.5 ms, repetition time (TR) = 20 ms, flip angle = 70°, slice thickness = 0.3 mm, field of view = 54 mm, number

of slices = 80–100, matrix = 180 × 180, acquisition plane = coronal; in-plane resolution = 300 × 300 μm^2, scan time ~ 5 min. The 70° flip angle used for the T1w-GRE sequence was selected as the result of an *in vivo* experiment on four C57BL/6 mice meant to identify the optimal flip angle for maximizing vascular contrast-to-noise ratio (CNR) due to our liposomal-Gd formulation (Fig. S1). T2-weighted (T2w) scans were acquired using a fast spin echo (FSE) sequence. Scan parameters for T2w-FSE scans were: echo time (TE) = 80 ms, repetition time (TR) = 6816 ms, slice thickness = 0.8 mm, field of view = 80 mm, number of slices = 33, matrix = 256 × 250, acquisition plane = coronal; in-plane resolution = 312.5 × 320 μm^2, number of excitations = 2, echo train length = 2, scan time ~ 6 min. The same T1w-GRE and T2w-FSE sequences were used in the post-contrast scans.

Coil calibrations were performed at the beginning of study at each time point and RF calibration and shimming were performed between each animal trial. Additionally, frequency calibration, transmitter gain adjustment, receiver gain adjustment, and dummy scans are automatically performed before each acquisition.

Five acquisitions were performed for each GRE scan protocol. The images from each of the acquisitions were qualitatively reviewed for motion artifacts. Magnitude-sum averages of GRE images were generated in Matlab® (version R2015a, MathWorks©, Natick, MA) using four acquisitions that showed minimal or no motion artifacts. Averaged FSE images were similarly generated in Matlab® using two FSE acquisitions.

2.4. Computed tomography (CT) imaging

High-resolution, contrast-enhanced CT imaging was used for secondary confirmation of MRI findings. One animal from each of the five timepoints (E10.5, E12.5, E14.5, E16.5, and E18.5), underwent CT within one hour following the completion of MRI. Imaging was performed on a small animal micro-CT system (Siemens Inveon). Animals were sedated with 3% isoflurane, setup on the CT animal bed, and then maintained at 1–2% isoflurane delivered using a nose cone setup. A pneumatically controlled pressure pad was placed underneath the animal's abdominal region to monitor respiration rate during the CT imaging session.

The scan parameters for the CT image acquisition were: 50 kVp, 0.5 mA, 850 ms X-ray exposure, 540 projections, 35 μm isotropic spatial resolution, scan time ~20 min. Contrast-enhanced CT imaging was performed after intravenous administration of a liposomal-iodinated blood pool contrast agent (1.65 mg I/g body weight).

2.5. Histology

Animals were euthanized after imaging and perfused with heparinized saline followed by a fixative to preserve uterine and fetal tissue. Individual feto-placental units (FPUs) were harvested and stored intact in 4% formalin. The FPUs were paraffin-embedded, cut into 8 μm thick sections and stained with Hematoxylin and Eosin (H&E). Histologic specimens were reviewed by a researcher experienced in mouse histopathology, including of the placenta, and a clinician experienced in the management of AIP.

2.6. Image analysis

Qualitative and quantitative analysis of MR images was performed in OsiriX (version 5.8.5, 64-bit) and MATLAB (version 2015a). Segmentation of feto-placental units on post-contrast T1w-GRE images was performed in ITK-SNAP (version 3.6.0, 64-bit) [23]. Regions-of-interest were manually drawn to segment the placenta (P), amniotic fluid (AF) compartment, and the retroplacental clear space (RPCS). 3D volumes were determined for the segmented structures and data presented as average and standard deviation.

2.6.1. Review of images

An abdominal radiologist with experience in placental imaging reviewed all post-contrast T1w-GRE scans. For each animal at each time point, averaged T1w-GRE images were reviewed for visualization of the retroplacental clear space. The visibility of the retroplacental clear space was scored for each FPU by the radiologist on a 3-point scale: 0 = not visible, 1 = partly visible and 2 = clearly visible. Data was presented as average and standard deviation of the scores.

2.6.2. Quantitative analysis

Signal-to-noise ratio (SNR) and contrast-to-noise ratio (CNR) were determined for target features in composite average images generated from four post-contrast T1w-GRE acquisitions. SNR for the placenta (SNR_P) was calculated according to Equation (1):

$$SNR_P = \frac{S_p}{N} \tag{1}$$

Here, S_P describes the mean signal within the placental volume of the composite average image while N describes the background noise of the composite average image, which was calculated as the standard deviation of a region of interest (ROI) placed in the background of the image. Retroplacental clear space SNR (SNR_R) was similarly determined using the mean signal within the RPCS volume, S_R. Sampling the background of the composite average image enables a common noise reference for comparing placental and RPCS SNR. CNR was then determined between the placenta and the retroplacental clear space according to Equation (2):

$$CNR = \frac{S_P - S_R}{N} \tag{2}$$

Which can also be expressed as the difference in SNR values calculated for the placenta (SNR_P) and RPCS (SNR_R). CNR values are not reported for E10.5 as the retroplacental clear space was not clearly visible. The Wilcoxon rank sum test was used for statistical analysis of placental, amniotic fluid, and retroplacental clear space volumes segmented from the post-contrast GRE images.

3. Results

Anatomical T2-weighted images demonstrated the growth and development of the feto-placental units over the course of the gestation (Fig. 1a–e). Due to high spatial resolution and contrast in the post-contrast T1w images, the placenta and amniotic fluid compartment were individually segmented to analyze volumetric changes during gestation. 3D volume renderings of the segmented placentae and amniotic fluid compartment indicated changes in feto-placental morphology between E10.5 and E12.5 and large increases in placental and fetal volumes during the latter stages of gestation (Fig. 1f–j). On the T1w-GRE scans, the placenta was not visible on the pre-contrast images due to poor contrast between the placenta and the amniotic fluid compartment (Fig. 2a–e). Post-contrast images clearly demonstrated the placenta as an avidly enhancing structure adjacent to the amniotic fluid compartment (Fig. 2f–j). The placental margin on the fetal side was clearly visible at all imaging time points. Enhancement was also seen in the myometrium, with an intervening hypointense region between the myometrium and the placenta, consistent with the retroplacental clear space (RPCS). The RPCS was visible starting at E12.5 and continued to be present throughout the rest of gestational period (Fig. 2). Quantitative signal analysis of the averaged post-contrast T1w images demonstrated higher signal-to-noise ratio (SNR) for the placenta (29 ± 4) than the RPCS (11 ± 0.4) throughout gestation (Fig. 3a). Placental SNR was highest at the final gestational timepoint, E18.5. The contrast-to-noise ratio (CNR) between the placenta and RPCS remained consistently high at all imaging time points of gestation (Fig. 3b). CNR was highest at E18.5 due to the higher placental SNR at the final gestational timepoint.

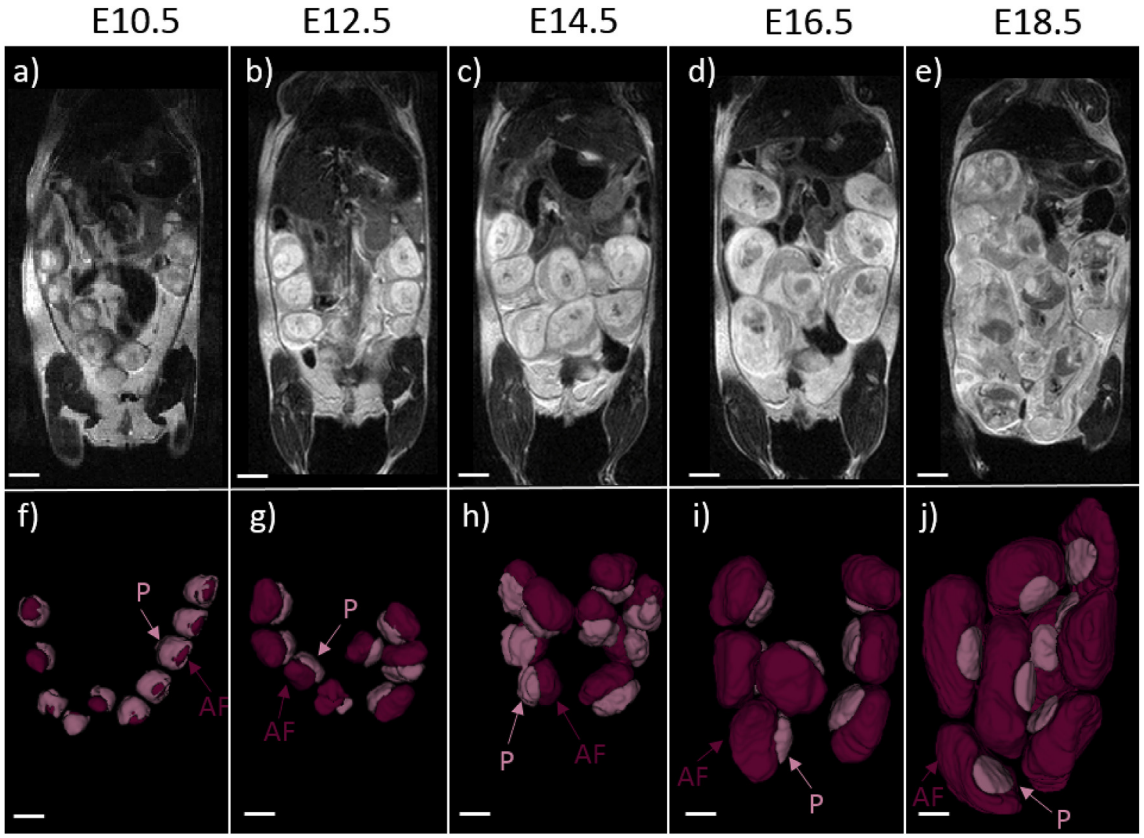

Fig. 1. T2-weighted anatomical images and 3D volume renderings from post-contrast T1-weighted MRI at each timepoint demonstrate feto-placental growth through gestation. (a–e) Representative T2-weighted, non-contrast coronal images of the mouse abdomen during pregnancy show progressive growth of the feto-placental units. (f–j) Analogous volume renderings of the segmented fetal compartment and placenta from contrast-enhanced T1-weighted MRI scans are provided at each of the five time points. Placenta (P) and the amniotic fluid (AF) components of the feto-placental unit are labeled. Scale bars in each figure represent 5 mm.

Radiologist review of post-contrast T1w images indicated that the visualization of the RPCS improved dramatically between E10.5 and E12.5 and continued to improve into the latter stages of gestation (Table 1). RPCS visualization was significantly different between E10.5 and all other time points ($p < 0.0005$). RPCS visualization was also significantly different between E12.5 and the later time points E14.5, E16.5, and E18.5 ($p < 0.05$) (Supplementary Material: Table S1).

The high SNR and CNR between placenta, RPCS and amniotic fluid compartment facilitated 3D segmentation and volumetric analysis of feto-placental features (Fig. 4). Placental volume progressively increased through gestation, however there was no significant difference between placental volume estimates on E16.5 and E18.5 ($p = 0.19$).

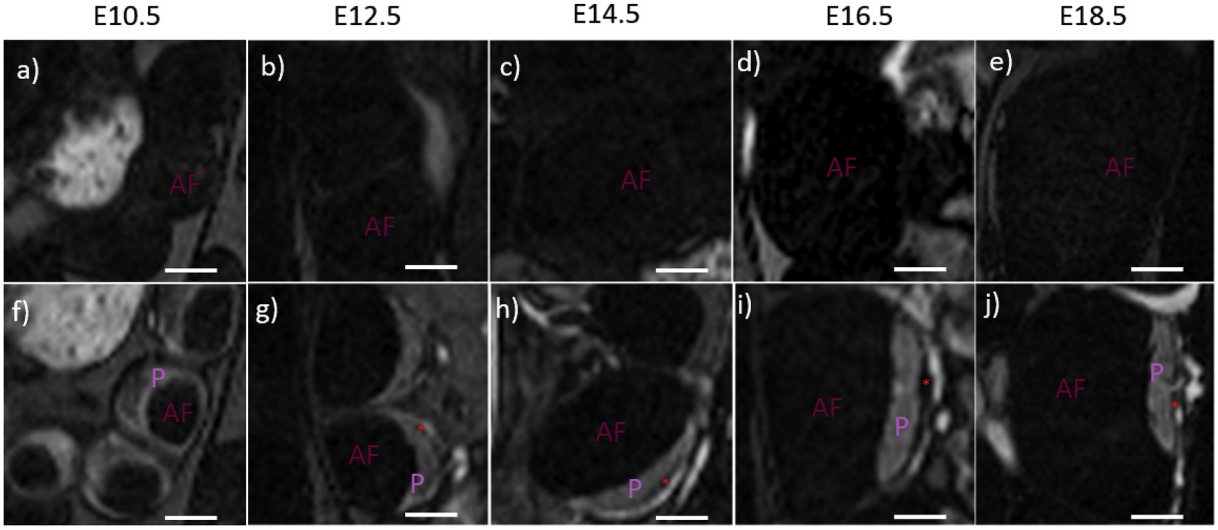

Fig. 2. T1-weighted pre and post-contrast images of individual feto-placental units demonstrate visibility of the retroplacental clear space (RPCS). (a–e) T1-weighted images without contrast have very low signal within the feto-placental unit. The placenta (P) and amniotic fluid (AF) of the fetal compartment are indistinguishable at all five gestational timepoints. (f–j) High signal is seen in the placenta and feto-placental vasculature in post-contrast T1-weighted images of the same animals. The RPCS (red asterisk) is visible starting on day 12.5 and is present at successive time points. Scale bars in each figure represent 3 mm.

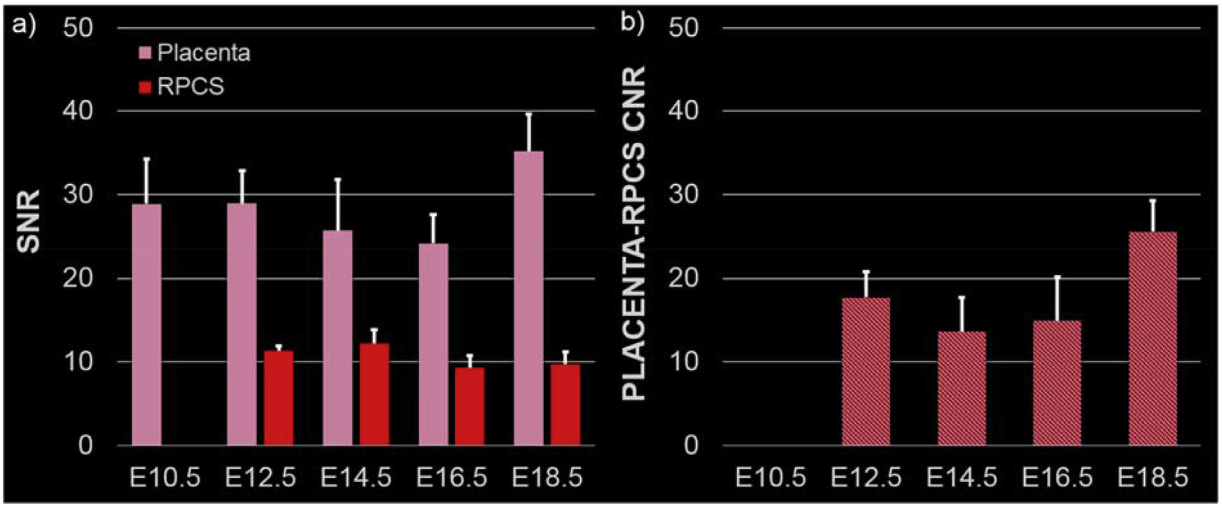

Fig. 3. Placenta and retroplacental clear space (RPCS) are well visualized on contrast-enhanced T1-weighted MRI. a) Signal-to-noise ratio (SNR) is calculated for the placenta (pink) and RPCS (red) at each of the five gestational time points. b) Contrast-to-noise ratio (CNR) between the placenta and RPCS is calculated at each of the five gestational time points. Error bars indicate standard deviation among fetal placental units at each time point.

Table 1
Score table for visualization of retroplacental clear space on post-contrast T1-weighted MRI images of feto-placental units (FPU) at different gestational time points. Visibility was scored by a radiologist on a scale of 0–2 with 0 assigned to not visible, 1 assigned to partly visible and 2 assigned to clearly visible. Scores are given as average and standard deviations for each time point with the median score reported in brackets: E10.5 (28 FPU), E12.5 (26 FPU), E14.5 (23 FPU), E16.5 (23 FPU), E18.5 (23 FPU).

	Radiologist Score (Mean ± STD); [Median]
E10.5	0.9 ± 0.3; [1]
E12.5	1.6 ± 0.5; [2]
E14.5	1.9 ± 0.4; [2]
E16.5	2.0 ± 0; [2]
E18.5	1.9 ± 0.3; [2]

Amniotic fluid compartment volume showed significant increases between all time points except between E12.5 and E14.5 ($p = 0.18$). The RPCS had poor visibility at E10.5 and therefore was not segmented. RPCS volume was relatively stable between E12.5 and E14.5 before increasing significantly at E16.5 ($p < 0.0005$). A significant decrease in RPCS volume was observed between E16.5 and E18.5 ($p < 0.0005$).

Contrast-enhanced CT imaging was performed at each time point to confirm MRI findings (Supplementary Material: Fig. S2). Consistent with MRI results, the placenta appeared as an enhancing structure relative to the non-enhancing amniotic fluid compartment and the RPCS. Furthermore, the visibility of RPCS progressively improved starting at E12.5, consistent with the MRI observations.

H&E staining of feto-placental tissue at the various gestational ages showed evidence of changes in uteroplacental architecture in the region of the RPCS as identified on MRI and CT (Fig. 5). The structure and morphology of the placenta exhibited dramatic changes between E10.5 and E12.5 days of gestation, whereby the placenta initially appeared globular and ovoid, and at the later time point showed a more characteristic crescent-shape. The placental shape did not change significantly between E12.5 and E18.5. On day 10.5, the placental mass was closely apposed to the myometrium (Fig. 5, panel a). Starting from E12.5, a lightly stained band between the myometrium and the labyrinth appeared in the region consistent with the RPCS as identified on imaging, which we will call the RPCS-zone on histology. Later time points (E14.5, E16.5) showed enlargement of the RPCS zone, similar to MR findings. The appearance of the RPCS zone at the final time point (E18.5) is substantially thinner, and more compressed in appearance, consistent with the lower volumetric estimate of the RPCS on MRI.

4. Discussion

Invasive placentation is characterized by loss of the fibrinoid layer between the myometrium and the placenta, and invasion of the syncitiotrophoblasts into the myometrial fibers. Loss of the fibrinoid layer in invasive placentation is thought to correlate with the lack of visualization of the retroplacental clear space (RPCS) as seen on antenatal ultrasound. Current imaging techniques for the visualization of RPCS suffer from poor sensitivity and specificity. Novel imaging techniques that allow consistent and reproducible visualization of RPCS could greatly aid in the diagnosis of placental invasion and serve as the first and crucial step in safe management of women with abnormally invasive placenta. In this pre-clinical study, we have characterized the visualization of the normal RPCS at different time points during gestation using MRI and a long circulating liposomal-Gd blood-pool contrast agent in a murine model.

The unique properties of liposomal-Gd enabled both qualitative and quantitative characterization of feto-placental development during gestation. Contrast-enhanced T1w-MRI demonstrated structural changes in placental development during the early part of gestation. The MRI findings were consistent with the histological observation of changes in placental morphology. The RPCS was clearly visible on contrast-enhanced T1w-MRI starting at E12.5 day of gestation. Radiologist review of contrast-enhanced T1w images indicated improvement in the visibility of the space as gestation progressed, though the space was marginally less clear at E18.5 than E16.5. Dynamic analysis of MRI-derived RPCS volume and microscopic analysis of H&E stained placental tissue corroborated the radiologist's image review for RPCS visualization. The thinner appearance and lower volume of the RPCS at E18.5 may be due to the growing fetus and amniotic compartment displacing the placenta towards the uterine wall or due to remodeling of the uteroplacental interface in preparation for placental detachment and expulsion after delivery. This is also consistent with the dramatic ~4-fold increase in amniotic fluid volume between E16.5 and E18.5 compared to ~1.2-fold increase in the placental volume.

Precision in volumetric estimates is dependent on image quality, which we demonstrate through our estimates of target feature SNR and CNR. The CNR between placenta and RPCS obtained in the current study is similar to our previous work [17]. However, the dose of liposomal-Gd agent used in the current study is ~33% lower than in the previous study [17]. The high CNR at lower dose of contrast agent is

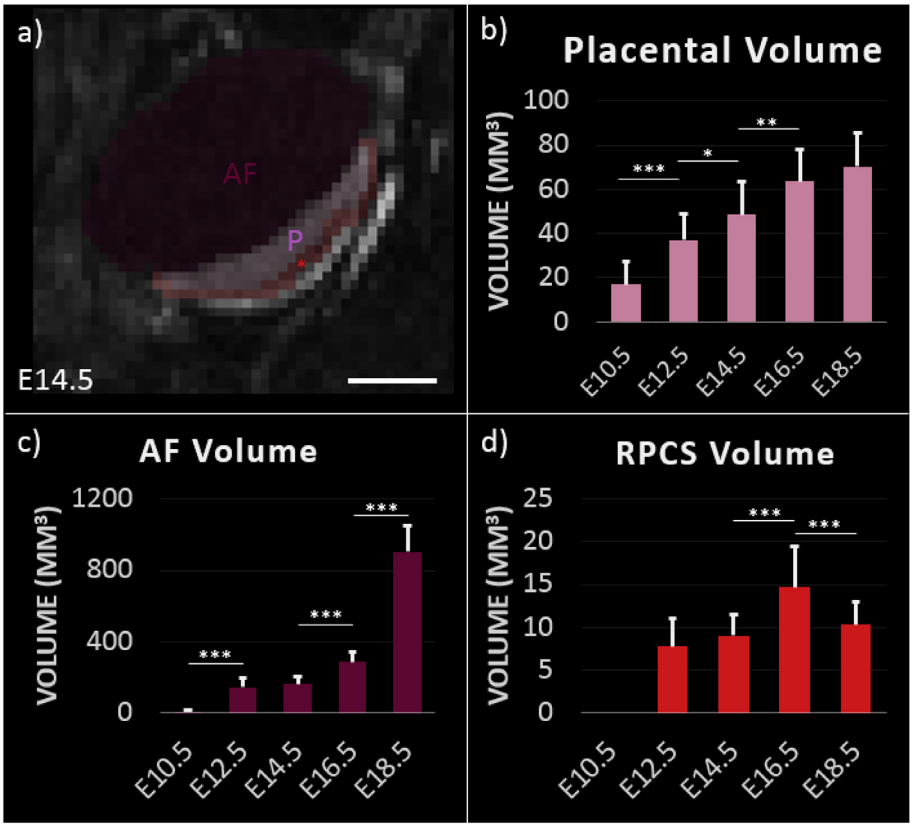

Fig. 4. Segmentation of contrast-enhanced T1-weighted MRI enables longitudinal monitoring of feto-placental development. a) Segmentation of feto-placental unit at day 14.5 of gestation. Placenta (P), amniotic fluid (AF), and RPCS (red asterisk) are labeled. Scale bar represents 3 mm. Volume estimates of b) placenta, c) amniotic fluid, and d) retroplacental clear space at each gestational time point are. Error bars indicate standard deviation among fetal placental units at each time point. Significance as determined by the Wilcoxon rank sum test are shown for $p < 0.05$ (*), $p < 0.005$ (**), and $p < 0.0005$ (***).

due to the higher T1 relaxivity (~6-fold higher compared to conventional Gd agents) of the modified liposomal-Gd construct, achieved by incorporating a macrocyclic DOTA-chelated Gd phospholipid conjugate into the liposomal bilayer [24].

The high CNR in post-contrast T1w images facilitated segmentation and analysis of volumetric changes in RPCS, placenta, and amniotic fluid compartment during gestation. While volume estimates of large features, such as placenta and amniotic fluid compartment, are less likely to be affected by partial volume averaging, volume estimate of small features, such as RPCS, may be affected by the current image spatial resolution (0.3 mm isotropic voxel). Image acquisition at higher spatial resolution is an alternative; however, this would come at the expense of longer scan time to compensate for higher noise levels. The use of a pregnant rat model with large feature sizes could be an option. However, the ease of generating clinically-relevant models of feto-placental pathologies in mice motivated us to perform the current study of RPCS characterization in a pregnant mouse model.

Some experimental limitations are acknowledged. The image acquisition did not include gating for motion due to maternal respiration, which can reduce image quality, even though animals were sedated with isoflurane. However, a major source of motion artifact when imaging pregnant animals is fetal movement, which cannot be

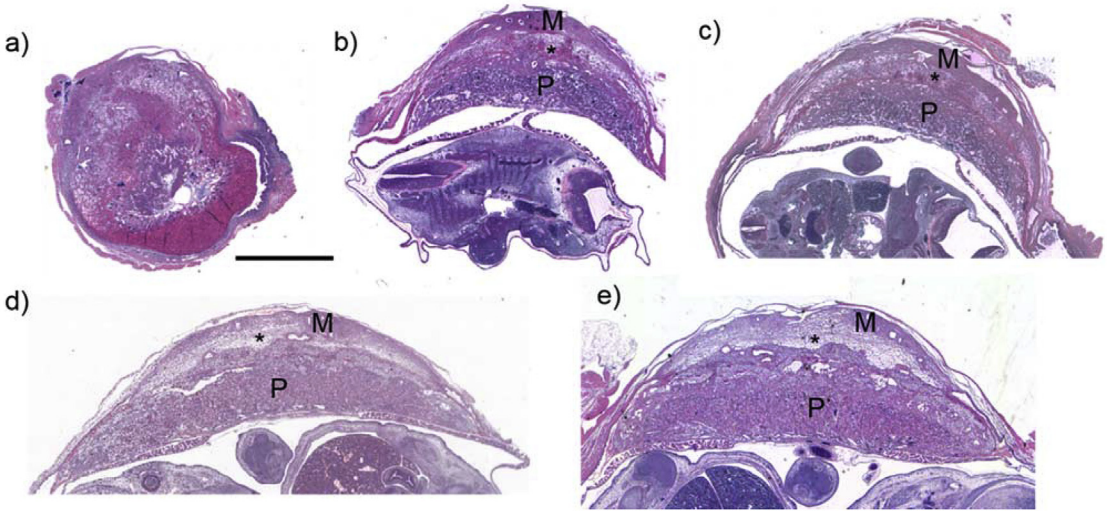

Fig. 5. Histology of feto-placental units show target features such as the placenta (P) myometrium (M), and RPCS (*). H&E stains of sectioned feto-placental units at a) 10.5, b) 12.5, c) 14.5, d) 16.5, and e) 18.5 days of gestation are shown. The asterisk (*) shows a spongiform, lightly stained band between the myometrium and the placental labyrinth, which corresponds to the retroplacental clear space (RPCS) as seen on imaging, or "RPCS Zone". Scale bar represents 2 mm.

externally controlled or gated for in scan protocol. To help diminish the overall effect of both respiratory and fetal motion artifact on image quality, multiple scans were acquired, and these were averaged externally as opposed to increasing the NEX in a single acquisition. The long blood circulating property of liposomal-Gd facilitates multiple acquisition with minimal changes in vascular signal. This approach allows us to discard scans with high degree of artifact; ultimately resulting in better feature conspicuity and the relatively high CNR values.

Another potential limitation of this study is the relatively few number of animals used at each time point. Three dams were included at each time point since the mice in our study typically bear anywhere from 7 to 10 feto-placental units each, thus resulting in 23–28 FPU per time point. Since the analysis is done at the FPU level and not the animal level, we decided three animals were sufficient at each time point, while minimizing the number of dams necessary to sacrifice.

Pre-clinical literature on the development and appearance of the RPCS is limited. To our knowledge, this is the first study describing the visualization and evolution of the RPCS in a pregnant rodent model. Future work will include efficacy testing of liposomal-Gd for the characterization of placental margins and retroplacental clear space in preclinical models of abnormal placentation, including invasive placenta.

Diagnosis of AIP with conventional ultrasound and MRI is challenging. An ideal detection method would be able to detect an absent or poorly defined RPCS, which would suggest invasive placenta. The use of a contrast agent that eliminates fetal gadolinium exposure, while enabling consistent and reproducible visualization of the RPCS and placental margins would be a significant advance in the field. The visualization of the retroplacental clear space appears with relatively consistent contrast-to-noise ratio at all time points after E12.5, indicating that liposomal Gd-enhanced MRI is a potentially more effective, feasible modality to define placental implantation and invasion than currently available options. If used in the context of invasive placentation therefore, we believe this agent will dramatically improve the sensitivity and specificity for detection of AIP.

Author contributions

Guarantor of integrity of entire study: A.V.A.; study concepts/study design or data acquisition or data analysis/interpretation: all authors; manuscript drafting or manuscript revision for important intellectual content: all authors; approval of final version of submitted manuscript: all authors; agree to ensure any questions related to the work are appropriately resolved: all authors; literature research: A.A.B, K.B.G., V.G., A.V.A, K.A.F.; experimental studies: A.A.B., K.B.G., I.S., L.D., Z.S.; statistical analysis: A.A.B., A.K., K.B.G.; manuscript editing, all authors.

Conflicts of interest

The authors have no conflicts to disclose.

Acknowledgements

The authors acknowledge the Texas Children's Hospital Small Animal Imaging Facility (SAIF) for micro-CT imaging; Texas Heart Institute Pathology Core for histology of feto-placental tissues; Prajwal Bhandari for assistance with imaging of H&E stained tissue sections. Financial support for this study was provided by National Institutes of Health (NIH) Grant No. R01 HD094347-01.

Appendix A. Supplementary data

Supplementary data to this article can be found online at https://doi.org/10.1016/j.placenta.2019.01.017.

References

[1] M.A. Belfort, Placenta accreta, Am. J. Obstet. Gynecol. (2010), https://doi.org/10.1016/j.ajog.2010.09.013.
[2] J.L. Bailit, W.A. Grobman, M.M. Rice, U.M. Reddy, R.J. Wapner, M.W. Varner, K.J. Leveno, J.D. Iams, A.T.N. Tita, G. Saade, D.J. Rouse, S.C. Blackwell, Morbidly adherent placenta treatments and outcomes, Obstet. Gynecol. (2015), https://doi.org/10.1097/AOG.0000000000000680.
[3] A.Y. Derman, V. Nikac, S. Haberman, N. Zelenko, O. Opsha, M. Flyer, MRI of placenta accreta: a new imaging perspective, Am. J. Roentgenol. (2011), https://doi.org/10.2214/AJR.10.5443.
[4] C.H. Comstock, R.A. Bronsteen, The antenatal diagnosis of placenta accreta, BJOG An Int. J. Obstet. Gynaecol. (2014), https://doi.org/10.1111/1471-0528.12557.
[5] C.H. Comstock, Antenatal diagnosis of placenta accreta: a review, Ultrasound Obstet. Gynecol. (2005), https://doi.org/10.1002/uog.1926.
[6] Z.S. Bowman, A.G. Eller, A.M. Kennedy, D.S. Richards, T.C. Winter, P.J. Woodward, R.M. Silver, Interobserver variability of sonography for prediction of placenta accreta, J. Ultrasound Med. (2014), https://doi.org/10.7863/ultra.33.12.2153.
[7] S.L. Collins, A. Ashcroft, T. Braun, P. Calda, J. Langhoff-Roos, O. Morel, V. Stefanovic, B. Tutschek, F. Chantraine, Proposal for standardized ultrasound descriptors of abnormally invasive placenta (AIP), Ultrasound Obstet. Gynecol. (2016), https://doi.org/10.1002/uog.14952.
[8] N. Zosmer, E. Jauniaux, C. Bunce, J. Panaiotova, H. Shaikh, K.H. Nicholaides, Interobserver agreement on standardized ultrasound and histopathologic signs for the prenatal diagnosis of placenta accreta spectrum disorders, Int. J. Gynecol. Obstet. (2018), https://doi.org/10.1002/ijgo.12389.
[9] F. D'Antonio, C. Iacovella, A. Bhide, Prenatal identification of invasive placentation using ultrasound: systematic review and meta-analysis, Ultrasound Obstet. Gynecol. (2013), https://doi.org/10.1002/uog.13194.
[10] K.E. Fitzpatrick, S. Sellers, P. Spark, J.J. Kurinczuk, P. Brocklehurst, M. Knight, The management and outcomes of placenta accreta, increta, and percreta in the UK: a population-based descriptive study, BJOG An Int. J. Obstet. Gynaecol. (2014), https://doi.org/10.1111/1471-0528.12405.
[11] L. Azour, C. Besa, S. Lewis, A. Kamath, E.R. Oliver, B. Taouli, The gravid uterus: MR imaging and reporting of abnormal placentation, Abdom. Radiol. (2016), https://doi.org/10.1007/s00261-016-0752-5.
[12] A. Kilcoyne, A.S. Shenoy-Bhangle, D.J. Roberts, R.C. Sisodia, D.A. Gervais, S.I. Lee, MRI of placenta accreta, placenta increta, and placenta percreta: pearls and pitfalls, Am. J. Roentgenol. (2017), https://doi.org/10.2214/AJR.16.16281.
[13] M.K. Shetty, D.K. Dryden, Morbidly adherent placenta: ultrasound assessment and supplemental role of magnetic resonance imaging, Semin. Ultrasound CT MRI (2015), https://doi.org/10.1053/j.sult.2015.05.007.
[14] American College of Obstetricians & Gynecologists, ACOG committee opinion no. 529: placenta accreta, Obs. Gynecol. (2012), https://doi.org/10.1097/AOG.0b013e318262e340.
[15] S.K. Goergen, E. Posma, D. Wrede, J. Collett, J. Pyman, E. Alibrahim, J. Keene, A. Dobrotwir, Interobserver agreement and diagnostic performance of individual MRI criteria for diagnosis of placental adhesion disorders, Clin. Radiol. (2018), https://doi.org/10.1016/j.crad.2018.05.021.
[16] A.E. Millischer, B. Deloison, S. Silvera, Y. Ville, N. Boddaert, D. Balvay, N. Siauve, C.A. Cuenod, V. Ttsatsaris, L. Sentilhes, L.J. Salomon, Dynamic contrast enhanced MRI of the placenta: a tool for prenatal diagnosis of placenta accreta? Placenta (2017), https://doi.org/10.1016/j.placenta.2017.03.006.
[17] K.B. Ghaghada, Z.A. Starosolski, S. Bhayana, I. Stupin, C.V. Patel, R.C. Bhavane, H. Gao, A. Bednov, C. Yallampalli, M. Belfort, V. George, A.V. Annapragada, Preclinical evaluation of a nanoparticle-based blood-pool contrast agent for MR imaging of the placenta, Placenta (2017), https://doi.org/10.1016/j.placenta.2017.06.008.
[18] T.J. Fraum, D.R. Ludwig, M.R. Bashir, K.J. Fowler, Gadolinium-based contrast agents: a comprehensive risk assessment, J. Magn. Reson. Imag. (2017), https://doi.org/10.1002/jmri.25625.
[19] J.G. Ray, M.J. Vermeulen, A. Bharatha, W.J. Montanera, A.L. Park, Association between MRI exposure during pregnancy and fetal and childhood outcomes, JAMA, J. Am. Med. Assoc. (2016), https://doi.org/10.1001/jama.2016.12126.
[20] A.N. Shetty, R. Pautler, K. Ghagahda, D. Rendon, H. Gao, Z. Starosolski, R. Bhavane, C. Patel, A. Annapragada, C. Yallampalli, W. Lee, A liposomal Gd contrast agent does not cross the mouse placental barrier, Sci. Rep. (2016), https://doi.org/10.1038/srep27863.
[21] K.B. Ghaghada, M. Ravoori, D. Sabapathy, J. Bankson, V. Kundra, A. Annapraganda, New dual mode gadolinium nanoparticle contrast agent for magnetic resonance imaging, PLoS One (2009), https://doi.org/10.1371/journal.pone.0007628.
[22] Ketan B. Ghaghada, Z. Starosolski, Igor Stupin, Saakshi Bhayana, Haijun Gao, Rohan C. Bhavane, Chandreshkumar Patel, Robia Pautler, Chandrasekhar Yallampalli, A.V. Annapragada, High-resolution placental MR angiography using a nanoparticle contrast agent, Int. Sociey Magn. Reson. Med. 2016.
[23] P. Yushkevich, J. Piven, H. Cody, S. Ho, User-guided level set segmentation of anatomical structures with ITK-SNAP, Neuroimage 31 (2006) 1116–1128, https://doi.org/10.1016/j.neuroimage.2006.01.015.
[24] K.B. Ghaghada, S. Z, I. Stupin, C. Patel, R.C. Bhavane, F. Leao-Barbosa, MR imaging of retroplacental clear space in a pregnant rat model, Radiol. Soc. North Am. Annu. Meet., Chicago, IL, 2017.